ChemPubSoc Europe

DOI: 10.1002/cssc.201402818

CHEMSUSCHEM Full Papers

Carbon Dioxide Splitting in a Dielectric Barrier Discharge Plasma: A Combined Experimental and Computational Study

Robby Aerts,* Wesley Somers, and Annemie Bogaerts*[a]

Plasma technology is gaining increasing interest for the splitting of CO_2 into CO and O_2. We have performed experiments to study this process in a dielectric barrier discharge (DBD) plasma with a wide range of parameters. The frequency and dielectric material did not affect the CO_2 conversion and energy efficiency, but the discharge gap can have a considerable effect. The specific energy input has the most important effect on the CO_2 conversion and energy efficiency. We have also presented a plasma chemistry model for CO_2 splitting, which shows reasonable agreement with the experimental conversion and energy efficiency. This model is used to elucidate the critical reactions that are mostly responsible for the CO_2 conversion. Finally, we have compared our results with other CO_2 splitting techniques and we identified the limitations as well as the benefits and future possibilities in terms of modifications of DBD plasmas for greenhouse gas conversion in general.

Introduction

In recent years, there has been a growing interest in the conversion of CO_2 into value-added chemicals or new fuels by means of plasma technology.[1–36] This includes both pure CO_2 splitting into CO and O_2[1–16] as well as the reaction with CH_4 (i.e., so-called dry reforming),[18–32] H_2,[33] or H_2O[35,36] to yield syngas and other useful products, such as methanol, formaldehyde, and formic acid. Different types of plasmas have been applied for this purpose, but most research is performed with dielectric barrier discharges (DBD),[1–6,10,18–25,27–30] microwave plasmas,[12,15,31] and gliding arc discharges. In this study, we focus on a DBD as it has a very simple design, which is beneficial for up-scaling for real applications. This was demonstrated many years ago for the large-scale production of ozone.[7,34] Moreover, it operates at atmospheric pressure, which is most suitable for practical applications. Finally, it can be combined easily with a packing (of simple dielectric beads and/or catalytic material),[2,21–25] which opens perspectives for the selective production of targeted compounds.

However, before the technology is ready for practical applications, a more systematic investigation of the optimum operating conditions is still needed. In spite of the many papers published, as mentioned above, such a systematic investigation for a DBD that focuses on conversion and energy efficiency under a wide range of conditions has not yet been performed. In the present study, this will be performed for the case of the splitting of pure CO_2 into CO and O_2.

[a] Dr. R. Aerts, W. Somers, Prof. Dr. A. Bogaerts
Department of Chemistry
University of Antwerp
Universiteitsplein 1, 2610 Wilrijk (Belgium)
E-mail: robby.aerts@uantwerpen.be
annemie.bogaerts@uantwerpen.be

Some scattered results on CO_2 splitting have been reported for specific operating conditions.[1–3] Paulussen et al.[1] investigated the effect of flow rate, applied power, frequency, and temperature and reported a maximum conversion of 30% at a flow rate of 0.05 L min^{-1}, a power density of 15 W cm^{-3}, and a frequency of 60 kHz. Yu et al.[2] found that the addition of a dielectric packing results in an increase of the conversion from 8 to 22.5% at a plasma power of 35.3 W and a flow rate of 40 mL min^{-1}. Tagawa et al.[3] proposed a hybrid reactor, that is, a DBD plasma on the surface of a solid oxide electrolyzer cell (SOEC) but they did not study the DBD without the SOEC in detail.

Some results are also reported for a mixture of CO_2 with an inert gas, for example, Ar and N_2.[4–6,37–40] Wang et al.[37] investigated the effect of the electrode material and concluded that a Cu electrode has the highest reactivity towards CO_2 decomposition. New ceramic dielectric barriers were developed by Li et al.[4,5,39,40] and Wang et al.,[6] which gave rise to an increase of the conversion. Zheng et al.[38] studied the effect of voltage and CO_2 concentration and found that a high voltage and a low CO_2 concentration gave rise to a lower energy efficiency.

Therefore, we believe strongly that a more systematic study is required to improve the performance and also to create a benchmark for other (plasma) technologies. The process we envisage is as follows [Eq. (1)]:

$$CO_2 \rightarrow CO + {}^1/_2\,O_2 \qquad \Delta H_R = 279.8\ \text{kJ mol}^{-1} = 2.9\ \text{eV molecule}^{-1}\ \ (\text{at } 300\ \text{K}) \tag{1}$$

This reaction is highly endothermic, so the energy efficiency of the process is a critical issue. However, plasmas can be beneficial for this purpose compared to other (classical) technologies as it is well known that the vibrational levels of CO_2 can

be populated efficiently in a plasma, and this forms an attractive, energy-efficient route for the dissociation of CO_2, as explained in detail by Fridman.[7] Moreover, plasma technology could also be very powerful for energy storage, which is a topic of great importance because of the increasing contributions of solar and wind energy in the electricity production portfolio. Indeed, these renewable energy sources give rise to peaks in electricity production, therefore, better storage capacities are urgently needed. Plasma technology is a very powerful candidate for this purpose because of its high flexibility and its capability to be switched on and off easily.[41]

In this paper, we have performed experiments by varying the applied frequency, power, gas flow rate, dielectric material, and discharge gap with a focus on the CO_2 conversion and energy efficiency. Moreover, we have performed computer simulations to elucidate the underlying mechanisms of the CO_2 splitting process. Finally, we compare our results with other CO_2 splitting techniques and we identify the limitations and future possibilities for CO_2 splitting by DBD plasmas.

Results and Discussion

Experimental parameter screening

In this section we will discuss the experimental results of the influence of various operating parameters, that is, frequency, kind of dielectric, discharge gap, electrical power, and gas flow rate, on the CO_2 conversion and energy efficiency of the process. We have also investigated the effect of these parameters on the selectivities of the formed products, that is, CO and O_2, but no influence was observed. The CO and O_2 selectivities were always around 50% under all conditions investigated. This is expected as the underlying chemistry of CO_2 splitting is very simple, that is, it is determined by the reaction: $CO_2 \rightarrow CO + {}^1/_2 O_2$. Some traces of O_3 can be formed (see reaction scheme and calculated number densities below) but this could not be detected in our GC analysis.

Effect of the frequency

The frequency (varied in the range between 6 and 75 kHz at a constant flow rate and plasma power) had a negligible influence on the conversion and energy efficiency. However, the plasma appears more filamentary at high frequency (75 kHz) compared to that at low frequency (6 kHz; Figure 1). Therefore, we apply a fixed frequency of 23.5 kHz in this study, which is the energetically optimal resonance frequency of the power generator used.

Effect of the dielectrics

We performed several experiments with different discharge gaps and under a wide range of operating conditions to compare quartz and alumina (99.7% Al_2O_3, Ceratec) as dielectrics but we observed no significant differences on the performance of the CO_2 splitting. The conversion and energy efficiency for both dielectrics as a function of specific energy input (SEI) for a discharge gap of 1.8 mm are shown in Figure 2 (see also Experimental Section). The SEI is defined here by changing the gas flow rate between 10 and 500 mL min^{-1} while the applied power is kept constant at 80 W. This results in a plasma power of (35 ± 3) W for quartz and (39 ± 1) W for alumina. The conversion increases with SEI, as expected, and reaches values up to 35% at the highest values of SEI investigated (around 225 J cm^{-3}, which corresponds in this case to a gas flow rate of 10 mL min^{-1} to a power of (39 ± 1) W or a quite long gas residence time of 44 s). The energy efficiency, however, decreases with a higher SEI, which is also expected (see Experimental Section). If a conversion of 35% is reached, the energy efficiency is only 2%. A higher energy efficiency of 8% could be reached at an SEI of 25 J cm^{-3}, but this corresponds to a very low conversion of only a few percent. Hence, there is a clear trade-off between conversion and energy efficiency. Depending on the targeted application and the boundary conditions (e.g., the use of sustainable electricity), one or the other can be optimized or a compromise between both can be sought.

Figure 1. Pictures of the DBD plasma at a frequency of A) 6 and B) 75 kHz to illustrate the difference in filamentary character.

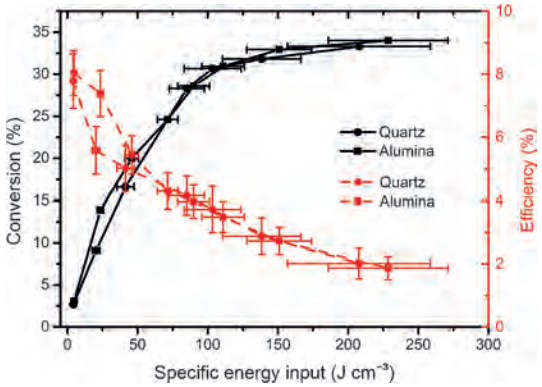

Figure 2. Effect of the dielectric on the conversion (black curves, left axis) and energy efficiency (red curves, right axis) as a function of the SEI. The calculation of the error bars is based on the uncertainties of the power, the flow rate, and the GC measurements. The error bars of the conversion in the *y* direction are smaller than 1% and, therefore, not visible.

Although virtually no difference was observed between quartz and alumina dielectrics on the conversion and energy efficiency (except for some minor differences in the lower region of the SEI, i.e., below 100 J cm^{-3}), the use of alumina instead of quartz has some advantages in terms of fabrication, and it is more resistant against arc formation and high temperature (melting point of 2054 vs. 1470 °C for quartz).[42] In the literature some more sophisticated dielectrics, such as $Ca_{0.8}Sr_{0.2}TiO_3$[6] and $Ca_{0.7}Sr_{0.3}TiO_3$ with 0.5 wt% $Li_2Si_2O_5$,[4,39] were reported to enhance the CO_2 conversion and/or energy efficiency because they increase the density of the filaments in the plasma. This effect is discussed more thoroughly below.

Effect of the discharge gap

The influence of the discharge gap on the conversion and energy efficiency is presented as a function of the SEI in Figure 3. We use here a quartz dielectric because it is transparent and thus allows visible observation. The SEI is varied by adjusting the gas flow rate from 10–500 mL min^{-1} at a constant plasma power of (35 ± 3) W.

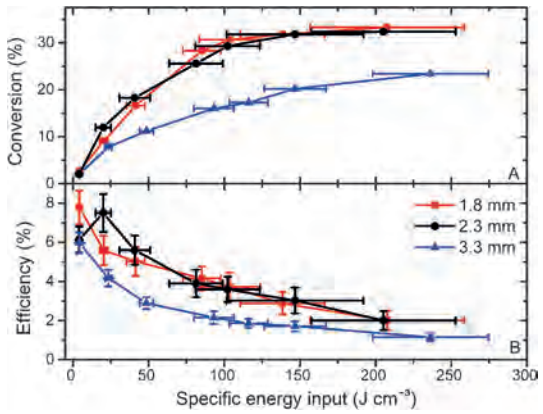

Figure 3. Effect of A) the discharge gap on the conversion and B) energy efficiency as a function of the SEI. The calculation of the error bars is based on the uncertainties of the power, the flow rate, and the GC measurements. The error bars of the conversion in the *y* direction are smaller than 1% and, therefore, not visible.

Gaps of 1.8 and 2.3 mm yield roughly the same conversion and energy efficiency, but a gap of 3.3 mm results in a clear decrease in the conversion and hence also in the energy efficiency. A larger gap of 4.5 mm was also tested, but the discharge was only ignited at the sharp edges of the foil electrode and thus no stable volume discharge was established.

For a fixed SEI (and hence gas flow rate and power), the residence time will be longer and the power density will be lower for the larger-discharge gaps because of the larger volume (i.e., the reactor volume is 7.4, 9.2, and 12.3 cm^3 for the gaps of 1.8, 2.3, and 3.3 mm, respectively). For instance, at an SEI of 100 J cm^{-3}, the residence times will be 22.1, 27.4, and 36.8 s and the power densities will be 4.7, 3.7, and 3.2 W with gaps of 1.8, 2.3, and 3.3 mm, respectively. It appears that this longer residence time and lower power density compensate for each other for the gaps of 1.8 and 2.3 mm, but the lower power density seems dominant for the 3.3 mm gap.

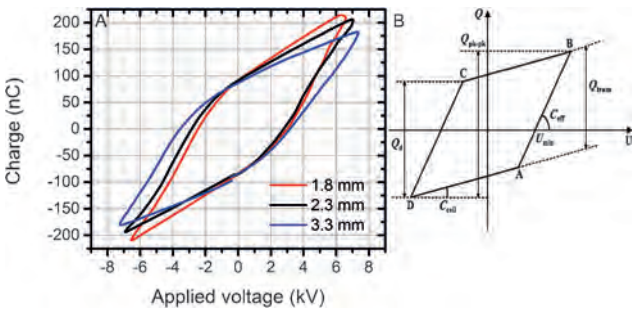

Figure 4. A) Lissajous plots for the three different discharge gaps at a plasma power of ≈35 W with a quartz dielectric and B) a schematic diagram of the Lissajous plot that explains all the quantities that can be deduced from it (see text).

Therefore, we make a more detailed analysis of the effect of the discharge gap by looking at the Lissajous plots (Figure 4). The total surface area is the same as it is determined by the plasma power (35 W), but nevertheless, there are distinct differences in the three Lissajous plots. Indeed, as the gap increases, a larger applied voltage is necessary to maintain the discharge (i.e., 13, 14, and 15 kV_{pp} for gaps of 1.8, 2.3, and 3.3 mm, respectively). Moreover, as the plasma power is the same, this increase in applied voltage is compensated by a decrease in peak-to-peak charge.

However, the difference in applied voltage and charges for the three discharge gaps is gradual and the same for the gaps of 1.8, 2.3, and 3.3 mm, therefore, this cannot explain why virtually no difference in conversion and energy efficiency was observed between 1.8 and 2.3 mm, whereas the difference was quite striking for the 3.3 mm gap. Therefore, to understand the effect of the gap on the conversion fully, we calculated the capacitance for the dielectric (C_d), the gap (C_g), and the reactor without plasma (C_{cell}) and the effective capacitance during the plasma-on stage (C_{eff}) [Eqs. (2)–(4)].[43]

$$C_d = \frac{2\pi \varepsilon_0 \varepsilon_d L}{\ln(r_{outer}/r_{inner})} \quad (2)$$

$$C_g = \frac{2\pi \varepsilon_0 \varepsilon_g L}{\ln(r_{inner}/r_{rod})} \quad (3)$$

$$C_{cell} = \frac{1}{C_d} + \frac{1}{C_g} \quad (4)$$

In these formulae $\varepsilon_0 = 8.854 \times 10^{-12}$ F m^{-1} is the permittivity of a vacuum, $\varepsilon_g = 1.000922$ is the relative permittivity of CO_2, and the relative permittivity of the dielectric tube (ε_d) is 3.8 for quartz.[43,44] Furthermore, L is the length of the plasma (90 mm; see above), r_{inner} and r_{outer} are the inner and outer radii of the dielectric tube (constant in the three cases), and r_{rod} is the radius of the high-voltage electrode (rod), which is varied at 5, 6, and 6.5 mm. This results in a constant C_d of 67 pF, whereas C_g varies from 21 pF for the smallest gap (1.8 mm) to 16 pF for the gap of 2.3 mm and 10 pF for the largest gap of 3.3 mm.

These values should be compared with the slopes of lines AB and CD from the Lissajous plots (Figure 4), which represent C_{eff} during the discharge-on phase if the gas breakdown occurs in the gap and the plasma is ignited. The slope of these lines should be equal to C_d for a gap bridged fully.[45] In our case, C_{eff} is determined to be 56 pF for the gaps of 1.8 and 2.3 mm and 40 pF for the gap of 3.3 mm. This is clearly lower than the capacitance of the dielectric quartz tube ($C_d = 67$ pF) especially for the largest gap, which indicates that the discharge gap is not bridged fully. Tu et al. reported that C_{eff} depends on the spatial distribution of the discharge across the gap over a half-period of the applied voltage.[25] Hence, it can be concluded that the total plasma volume (i.e., the volume occupied by the streamers) is much smaller than the total volume of the plasma reactor, especially for the largest gap.

This reduced formation of streamers is clearly visible in the electric current waveforms (Figure 5). If we compare the waveforms of the 1.8 and 2.3 mm gaps, the absolute values of the current are somewhat lower for the 2.3 mm gap, which is correlated with the slightly lower peak-to-peak charges illustrated in the Lissajous plots. This trend is also continued and even more striking for the gap of 3.3 mm, but on top of that, the streamer frequency is clearly reduced compared to the gaps of 1.8 and 2.3 mm.

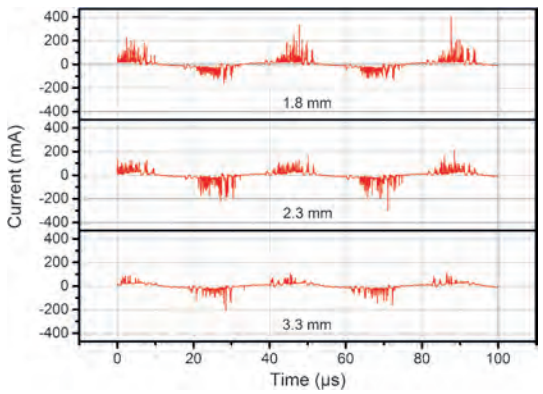

Figure 5. Comparison of the electric current waveforms for the three different discharge gaps at a plasma power of ≈35 W with a quartz dielectric to illustrate the reduced streamer formation for the gap of 3.3 mm.

To conclude, the gaps of 1.8 and 2.3 mm yield more or less the same CO_2 conversion and energy efficiency because they exhibit the same streamer behavior. However, the larger gap of 3.3 mm results in a significantly lower CO_2 conversion and energy efficiency (Figure 3) as less streamers are formed for a fixed SEI, which gives rise to a lower effective plasma volume and, therefore, a reduced possibility for CO_2 conversion. Moreover, the streamers seem to have lower peak currents, which corresponds to a decrease in the electron density according to Equation (5):

$$n_e = \frac{J}{E\,\mu_e\,e} \quad (5)$$

in which J is the current density, E is the electric field, μ_e is the electron mobility, and e is the elementary charge. Consequently, the lower electron density results in a lower CO_2 conversion because of the decrease in electron impact reaction rates.[10] Finally, an increasing gap gives rise to a reduced electric field strength (E/N), which results in a decrease of the average electron energy in the discharge. This lower electron energy (or reduced electric field) will affect the fraction of energy transferred to the various types of collisions.[10,46] Nevertheless, as the gap of 3.3 mm shows a lower conversion and energy efficiency than the gaps of 1.8 and 2.3 mm, we can conclude that the reduced streamer density in the 3.3 mm gap is more important to determine the lower conversion and energy efficiency than the other two effects.

Effect of the electric power and gas flow rate

As indicated by the formulae in the Experimental Section, the SEI in the plasma system is defined by both the gas flow rate and the plasma power. In the literature, the SEI is often used as a major determining factor for the conversion and energy efficiency, and therefore, the conversion and energy efficiency are often plotted as a function of SEI.[8,18,36,47] However, we observed that the same values of SEI defined by different combinations of plasma power and gas flow rate can result in different conversions. Therefore, in this section we investigate the influence of gas flow rate (or residence time) and plasma power on the CO_2 conversion and energy efficiency separately. To the best of our knowledge, such a separate study has not been published before.

The conversion and energy efficiency are plotted versus SEI for different values of residence time (or gas flow rate) at fixed plasma power (red curve) and for different values of plasma power at fixed gas flow rates (blue and black curves) in Figure 6. The plots indicate clearly that these two parameters affect the SEI and, therefore, the CO_2 conversion and energy efficiency, in different ways. In all cases, the conversion first increases with SEI but then reaches a maximum value, which appears to be different in the different cases. A low plasma power (40 W) with a low gas flow rate (10 mL min^{-1}, which corresponds to a long residence time of 44 s) gives rise to a maximum conversion (red curve). The same SEI can also be obtained with a higher plasma power and higher gas flow rate (or shorter residence time), and this results in a lower maximum conversion, which is clear from the black and blue curves. Hence, the flow rate (or gas residence time) seems to have a more pronounced effect on the conversion than the plasma power. The same effect is visible for the energy efficiency but it is less pronounced. To the best of our knowledge, this effect has not been reported before. It suggests that by tuning the plasma power and the gas flow rate, we can increase the conversion and energy efficiency at a certain SEI, which is very promising. However, this effect is only observed for high values of SEI (above 100 J cm^{-3}), which unfortunately gives rise to a low energy efficiency.

To compare the three cases presented in Figure 6 from an electrical point of view, the current and voltage waveforms for

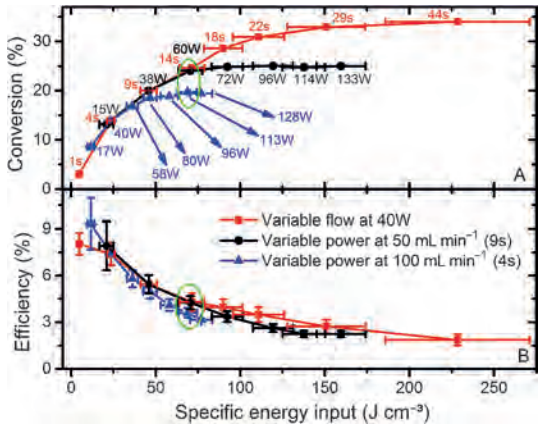

Figure 6. Effect of the gas flow rate (or residence time) and plasma power on A) the conversion and B) the energy efficiency plotted as a function of the SEI using alumina dielectrics. The corresponding values of plasma power that result in certain SEI values at fixed gas flow rates of 50 and 100 mL min^{-1} (black and blue curves) and the corresponding values of the residence time that result in certain SEI values at a fixed plasma power of ≈40 W (red curve) are also shown in A. The calculation of the error bars is based on the uncertainties of the power, the flow rate, and the GC measurements. For the sake of clarity, the error bars are only presented for the energy efficiency. The green circle in A indicates the conditions plotted in Figure 7.

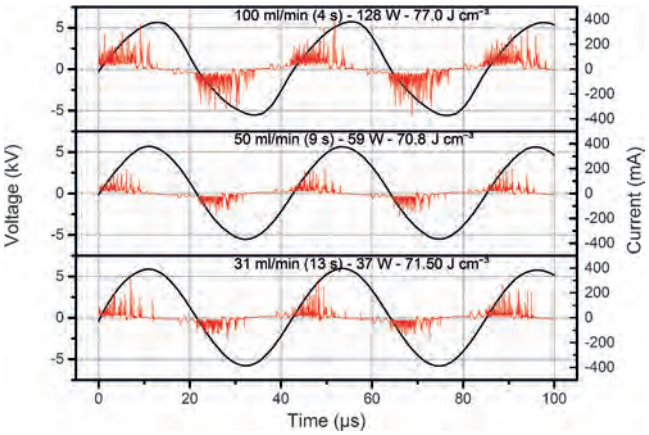

Figure 7. Comparison of the voltage and electric current waveforms for three different combinations of plasma power and gas flow rate (or residence time) that yield a similar SEI (cf. the green circle indicated in Figure 6).

three distinct combinations of plasma power and gas flow rate, which result in nearly the same SEI of 70 J cm^{-3}, are shown in Figure 7. We observe more streamers and especially higher current values in the case of a high power and high flow rate (top) than in the case of a low power and low flow rate (bottom), which is logical. Nevertheless, the first condition gives rise to a lower conversion. This indicates that a longer residence time, which arises from a lower gas flow rate (bottom) has a more pronounced effect on the conversion (and hence energy efficiency) than the higher power (and thus higher current and higher streamer intensity). Indeed, a longer residence time means that the CO_2 molecules can stay longer within the streamers, which seems to be more important for the conversion than the higher streamer intensity (or electron density) for the same SEI.

Modeling the plasma chemistry of CO_2 splitting

In this section we extend our model published previously[10] to longer residence times by simulating a large number of consecutive pulses (i.e., microdischarge filaments or streamers) at a frequency of 34.4 Hz chosen arbitrarily (see also the description of the model) until a given residence time is reached. As indicated above, the effective volume occupied by the sum of all individual microdischarges is much smaller than the total plasma reactor volume. Therefore, the power density used as input in our model, from which the SEI is calculated, is multiplied by a factor of seven to account for this. We do not know the exact value of the effective plasma volume occupied by the streamers, so this factor of seven is chosen somewhat arbitrarily because it yields reasonable agreement between the calculated and measured values for the CO_2 conversion (see below). Nevertheless, even if this factor can be considered as a kind of fitting parameter, it does have a physical meaning as demonstrated by Motret et al.[48,49] Even if the quantitative calculation results might be dependent on this factor, the qualitative trends predicted by the model can still be validated in this way, and the validated model can subsequently be used to elucidate the underlying plasma chemistry. This will be illustrated in this section, based on a reduced plasma chemistry, which still describes the essential processes for the CO_2 conversion and will be very useful for the development of time-consuming 2D or 3D plasma chemistry models.

Validation of the model

A comparison of the calculated conversion with measured values for different powers and gas flow rates as a function of SEI is illustrated in Figure 8 (cf. Figure 6). A very good agree-

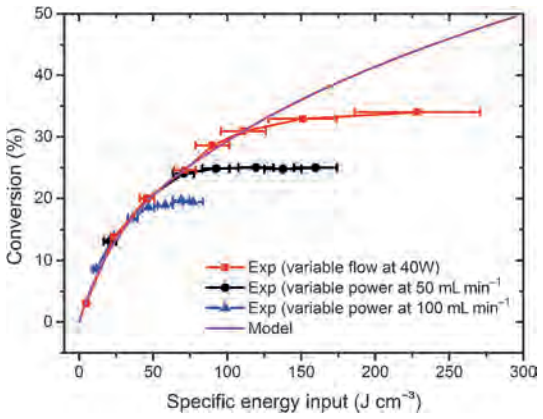

Figure 8. Comparison of the calculated and measured values for the conversion as a function of the SEI. Notably, the power density, and hence the SEI, used in the model is multiplied by a factor of seven to account for the lower volume occupied by the streamers (see text). The calculation of the error bars is based on the uncertainties of the power, the flow rate, and the GC measurements. The error bars in the *y* direction are smaller than 1% and, therefore, not visible.

ment is reached for SEI values up to 100 J cm^{-3}. Above 100 J cm^{-3}, the model does not show saturation, as in the experiments, but the experimental data also yield different degrees of saturation, which depends on the combination of power and gas flow rate, as explained in detail in above. However, the energy efficiency at these high SEI values is very low and the residence time becomes quite long, so these conditions are probably not attractive anyway. Therefore, we may conclude that the agreement between model and experiments is reasonable, at least in the SEI region of the most practical interest. Previously, we have checked that the calculated electron density and temperature in the model are in the correct order of magnitude compared with literature data.[10] Hence, we conclude that the model is sufficiently realistic to be used to elucidate the underlying chemical pathways of CO_2 splitting.

Reduced chemistry set for CO_2 splitting

As mentioned in the Experimental Section, the complete model contains 42 species that interact with each other in 501 chemical reactions. This will be prohibitive for 2D and 3D plasma models. Therefore, we have reduced the chemistry set described previously[10] based on the most important production and loss processes of our full model so that it only includes the most critical plasma species and reactions for the CO_2 splitting.

The comparison between the conversions calculated by the full model and the reduced model as a function of SEI is illustrated in Figure 9. A good agreement is reached in the lower

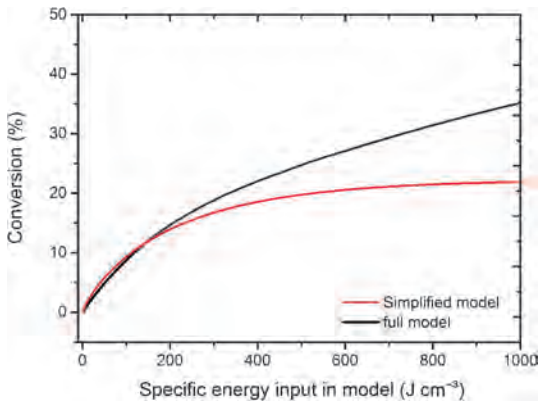

Figure 9. Comparison of the conversion, calculated with the simplified model and the full model from Aerts et al.,[10] as a function of SEI in the model. The simplified model is calculated from reactions 1 to 17 shown in Table 1.

range of the SEI, which yields a limited conversion of CO_2 (up to 15%) for the reasons discussed below. If the conversion rises above 15%, the chemistry becomes more complex because of the higher concentrations of CO and O_2. To obtain a good correlation in the higher SEI range, too many reactions have to be included so that there is no significant saving compared with the full model. Therefore, for higher conversions, we recommend the use of the full chemistry set. Only nine different species are included in this reduced model, namely, CO_2, CO, O, O_2, and O_3 as neutral species and CO_2^+, O_2^-, O^-, and the electrons as charged species. Indeed, we do not include vibrationally or electronically excited levels of the molecules as separate species. Although vibrationally excited CO_2 molecules play a critical role in the CO_2 splitting in microwave or gliding arc plasmas,[7,50] their contribution in DBD plasmas is of minor importance.[7,10,50] However, these excited species play a role in the consumption of the electron energy. To compensate for this, we included some dummy reactions with no change in chemical species to account for the energy loss in the electron energy equation.

The only electron impact ionization process included in the reduced model is the ionization of CO_2 to CO_2^+ (reaction 1 in Table 1), as this reaction was found to be much more important than the dissociative ionization of CO_2.[10] Moreover, the ionization processes of CO and O_2 are also less important as long as the conversion is not too high. This will of course limit the validity of the reduced model at low conversions (up to 15%; Figure 9), but the inclusion of these ionization processes will increase the number of species and reactions. Hence, this shows the trade-off between complexity (or calculation time) and the validity of the model. Furthermore, charge transfer processes between ions are not considered as the role of ions in the actual splitting of CO_2 is almost negligible.[10] The only reactions of the CO_2^+ ions included are recombination with electrons and O_2^- ions (reactions 11 and 12 in Table 1).

Three electron impact dissociation reactions are incorporated for CO_2, O_3, and O_2 (reactions 2, 4, and 5 in Table 1). The dissociation of CO can be neglected because it requires 1069.2 kJ mol^{-1}, whereas the dissociation of CO_2 requires 529.8 kJ mol^{-1}.[38] As a result of this energy difference, the total rate of CO dissociation, as calculated by the full model, is

Table 1. Reactions included in the reduced chemistry model and the corresponding rate coefficients. The rate coefficients are in units of cm^3 s^{-1} for the two-body reactions and in cm^6 s^{-1} for the three-body reactions.

Entry	Reaction	Rate coefficient	Ref.
1	$e^- + CO_2 \rightarrow CO_2^+ + 2e^-$	5.4×10^{-11}	[10][a]
2	$e^- + CO_2 \rightarrow CO + O + e^-$	5.8×10^{-11}	[10][a]
3	$e^- + CO_2 \rightarrow CO + O^-$	7.0×10^{-12}	[10][a]
4	$e^- + O_3 \rightarrow O + O_2 + e^-$	2.0×10^{-9}	[10][a]
5	$e^- + O_2 \rightarrow O + O + e^-$	2.0×10^{-9}	[10][a]
6	$e^- + O_2 \rightarrow O + O^-$	4.0×10^{-11}	[10][a]
7	$e^- + O_2 + M \rightarrow O_2^- + M$	3.0×10^{-30}	[10][a]
8	$O^- + CO \rightarrow CO_2 + e^-$	5.5×10^{-10}	[51]
9	$O^- + O_2 \rightarrow O_3 + e^-$	1.0×10^{-12}	[52]
10	$O^- + O_3 \rightarrow O_2 + O_2 + e^-$	3.0×10^{-10}	[53]
11	$e^- + CO_2^+ \rightarrow CO + O$	6.5×10^{-7}	[54]
12	$O_2^- + CO_2^+ \rightarrow CO + O_2 + O$	6.0×10^{-7}	[55]
13	$O + O + M \rightarrow O_2 + M$	$5.2\times10^{-35}\ \exp(900/T[K])$	[56]
14	$O + O_2 + M \rightarrow O_3 + M$	$4.5\times10^{-34}\ (T[K]/298)^{-2.70}$	[57]
15	$O + O_3 \rightarrow O_2 + O_2$	$8.0\times10^{-12}\ \exp(-17.13/T[K])$	[57]
16	$O + CO + M \rightarrow CO_2 + M$	$1.7\times10^{-33}\ \exp(-1510/T[K])$	[58]
17	$O_3 + M \rightarrow O_2 + O + M$	$4.1\times10^{-10}\ \exp(-11\,430/T[K])$	[51]

[a] Rate coefficient calculated by an online Boltzmann solver in the model at initialization conditions of pure CO_2.

much lower than the rate of CO_2 dissociation, especially for lower conversions (below 15%). Furthermore, three electron attachment processes are considered, that is, dissociative attachment to CO_2 and O_2 and (three-body) attachment to O_2 to produce O^- or O_2^- ions, respectively (reactions 3, 6, and 7 in Table 1). As only a limited number of reactions are included for these negative ions in the simplified model, this is another reason why the model should not be used for conversions above 15%. However, the electron attachment reactions with O_2 are essential, even in this reduced chemistry set, as they are faster than that with CO_2 and they will induce a decrease in electron density to result in a flattening in the CO_2 conversion upon increasing SEI, which is also observed experimentally (see above) because less electrons will be available for the direct splitting of CO_2. Furthermore, three electron detachment reactions are included, that is, by O^- upon collision with CO, O_2, and O_3 (reactions 8–10). The O_2^- ions, however, are neutralized by recombination with CO_2^+ ions (reaction 12; see above).

Finally, some chemical reactions between the neutral species are incorporated (reactions 13–17). The O atoms recombine almost completely to O_2 through reaction 13, although some O atoms give rise to the production of O_3, predominantly by reaction 14. Moreover, some O atoms can recombine with CO to produce CO_2 (reaction 16), especially at high conversions and long residence times. Indeed, this reaction will become important if the density of atomic oxygen is high enough. In addition, an increase in the supplied energy will also increase the rate of this reaction, for example, if a large fraction of O atoms is in excited levels or at higher gas temperature.[7] This is why the gas needs to be quenched (cooled) rapidly in thermal (or warm) plasmas used for CO_2 splitting to prevent the backward reaction (i.e., the recombination of CO and O to form CO_2 again).[7] Under our conditions, the gas temperature did not increase during splitting, that is, the gas temperature remains close to room temperature, and therefore, this reaction will be less important, at least for not excessively long residence times (see below). Hence, once the CO molecules are formed, they will be rather stable in the plasma. However, we do observe a certain balance in our model between O_3 and O_2 (reactions 13–15 and 17). However, the rate constants for the three-body reactions adopted from the literature show a variation between different publications and thus the exact O_3/O_2 ratio obtained by the model is subject to uncertainty. Experimental measurements of the O_3 density would give vital information to understand the balance between O_2 and O_3 in the splitting of CO_2. However, we were not able to detect O_3 with our GC setup.

The reactions included in the reduced model, the corresponding rate coefficients, and the references from which these data are adopted are listed in Table 1, and a schematic diagram of the reaction scheme is presented in Figure 10.

It is clear from Figure 10 that the actual splitting of CO_2 is quite straightforward. The most important reactions for CO_2 splitting are electron impact dissociation (to form CO and O atoms; reaction 2), electron impact ionization (to form CO_2^+ ions (reaction 1), which will further recombine dissociatively with electrons or O_2^- ions into CO and O and/or O_2; reactions 11 and 12), and electron dissociative attachment (to form CO and O^- ions; reaction 3). These three mechanisms contribute typically 43, 46, and 11% to the CO_2 splitting, respectively. As mentioned above, the CO molecules are relatively stable and will only react further at longer residence times or higher O densities; they can recombine with O^- ions (electron detachment of O^-; reaction 8) or O atoms (reaction 16) to reform CO_2. To analyze the importance of these backward reactions as a function of the residence time, the time-averaged rates (i.e., averaged over one pulse) are plotted in Figure 11 together with the time-averaged rates of the dominant loss processes of CO_2, that is, electron impact ionization, dissociation, and dissociative attachment.

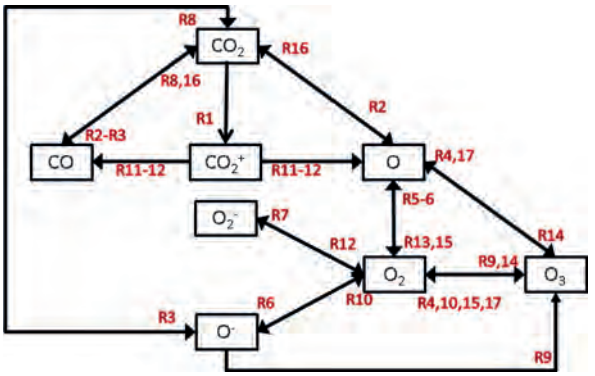

Figure 10. Reaction scheme to illustrate the chemistry of CO_2 splitting and further reactions as predicted by the reduced model.

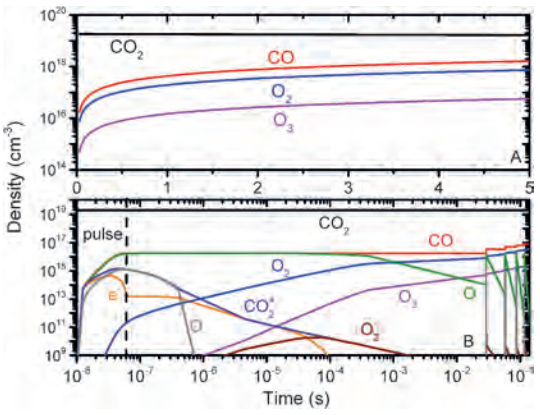

Figure 11. Time-averaged rates of the dominant loss processes of CO_2 (full lines) and the backward reactions of CO with O and O^- (dashed lines) calculated with the simplified model as a function of residence time for an SEI of 129 J cm^{-3}.

At a residence time of 0.5 s, both backward reactions are more or less equally important with a rate of 6×10^{16} cm^{-3} s^{-1}, but the sum of their rates is a factor of 4.5 lower than the sum of the rates of the main loss mechanisms of CO_2 (i.e., ionization, dissociation, and dissociative attachment). However, at a residence time of 5 s, the total rate of the backward reactions is only a factor of two lower than the total loss rate, which indicates that the backward process then becomes important. It is clear that the reaction with O^- ions has a more or less con-

stant rate of 6×10^{16} cm^{-3}s^{-1}, independent of the residence time, which is caused by the constant production of O^- ions from electron impact dissociative attachment with CO_2 (reaction 3). In contrast, the rate of the reaction with O atoms increases by almost an order of magnitude to 2×10^{17} cm^{-3}s^{-1} at 5 s. This can be explained by the increasing O_2 density and, therefore, the increasing production of O atoms by electron impact dissociation of O_2 (reaction 5). Overall, integrated over the residence time of 5 s, the total contribution from the recombination of CO with O atoms to the CO_2 production is 65%, and the recombination with O^- ions only contributes for 35%. Hence, we can distinguish two major phenomena that cause the flattening of the conversion at long residence times or high values of the SEI. The first is the decrease in the electron density caused by electron attachment with oxygen. The second is the increasing contribution of the backward reaction, that is, the recombination of O atoms with CO to reform CO_2.

At shorter residence times, however, the O atoms will recombine into O_2 or O_3 almost immediately (reactions 13 and14), and there are several other reactions between O, O_2, and O_3 as well (which sometimes also involve the negative ions; i.e., reactions 4–7, 9, 10, 15, and 17). Therefore, the most freedom to influence the splitting process can be found in the balance of $O/O_2/O_3$. Moreover, the introduction of H-containing gases, such as H_2 or CH_4, can further control the production of O_2 by the consumption of O atoms.[59]

To conclude, the selectivity towards CO will always be close to 50%, whereas the selectivity towards O_2 was predicted in the model to be between 45 and 50%, which depends on the O_3 production (if we keep in mind the uncertainties in the three-body rate coefficients, as mentioned above). The question is whether O_2 or O_3 would be the most valuable product. Based on the chemical reactivity, O_3 is more favorable, but because of its high reactivity, the storage of O_3 is not straightforward and, therefore, on-site production would be beneficial if O_3 is intended to be produced for bleaching or oxidizing purposes.[60]

Finally, the calculated number densities of the molecules included in the model are plotted as a function of residence time for an SEI of 129 J cm^{-3} (Figure 12(A)). It is clear that the CO_2 density decreases gradually as it is converted into CO and O_2 and a fraction of O_3. The densities of the other species included in the model (i.e., the O atoms and the various ions) are negligible on these long timescales; however, their densities are plotted together with the molecule densities as a function of time during five consecutive microdischarge pulses (which mimic the filaments in the DBD reactor) in Figure 12(B) for the same SEI value. We use a logarithmic *x* axis to illustrate the temporal behavior of the ions during and after one pulse. It is clear that the densities of CO, O_2, and O_3 increase (more or less) stepwise at each pulse, whereas the CO_2 density decreases slightly. The densities of the O atoms, the various ions, and the electrons increase during each pulse but they decay again before the next pulse is reached. The decay time is the longest for the O atoms, whereas the electrons and the various negative ions become completely negligible long before the next pulse starts.

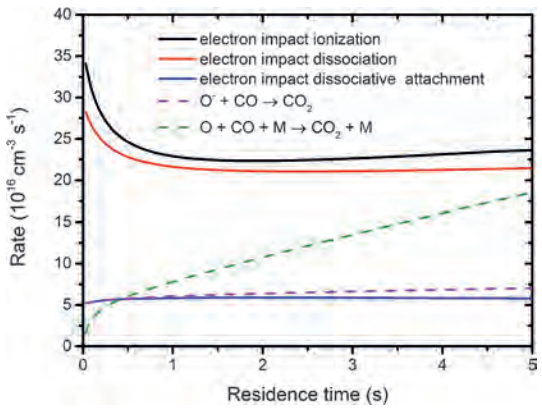

Figure 12. A) Calculated molecule densities as a function of residence time and B) densities of all plasma species included in the simplified model as a function of time during five consecutive microdischarge filaments for an SEI of 129 J cm^{-3}.

Theoretical energy cost versus actual energy cost

In our experiments, the conversion was at maximum around 35% but this was reached at a high SEI above 200 J cm^{-3}, and therefore, it corresponds to a low energy efficiency of only 2%. A maximum energy efficiency of 8% could be obtained at a low SEI (~25 J cm^{-3}) at the expense of the conversion, which was only a few percent in this case. An important remark is that the energy efficiency reported in our work, as well as that in the literature, is calculated with respect to the plasma power. Therefore, we should refer to it as the "energy efficiency of the plasma" or the "theoretical energy efficiency". Indeed, the plasma power is typically around 50% lower than the applied electrical power in a DBD reactor because of losses in the high-voltage power source and the cables (reflection, heating, zero-load power requirements, etc). Consequently, the energy efficiency of the process will be lower or vice versa the energy cost will be higher.

A comparison of the energy cost and the energy efficiency calculated from the electrical power and the plasma power as a function of the SEI is shown in Figure 13. It is clear that the

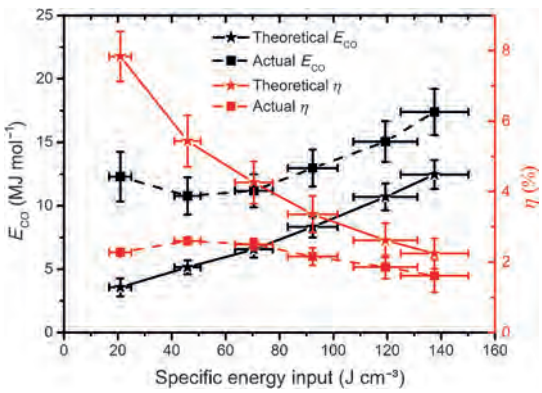

Figure 13. Energy cost (black curves; left axis) and energy efficiency (red curves; right axis) calculated from the electrical power (actual; dashed lines) and from the plasma power (theoretical; solid lines) as a function of the SEI using alumina dielectrics and a constant flow rate of 50 mL min^{-1}.

actual energy cost, calculated from the electrical power, is at least 50% higher (black dashed line) and, therefore, the actual energy efficiency (red dashed line) is also at least 50% lower, that the theoretical energy cost and energy efficiency (black and red solid lines).

At high SEI values, the difference between the actual and theoretical energy cost and energy efficiency is somewhat lower than that at low SEI values. This can be explained by the zero-load power of the power source, which is $\approx$40 W in our experiments, independent of the applied power. Hence, the power loss at a high applied power is thus smaller than at a low applied power.

In this paper, we focus on the energy efficiency of the plasma process itself, as is typical of plasma studies in the literature. Nevertheless, the total electrical power consumption must be kept in mind, especially if different plasma sources are compared, and certainly if other CO_2 conversion technologies are compared.

Feasibility of CO_2 splitting by DBDs and comparison with other techniques

The purpose of this study is to identify the possibilities and drawbacks of CO_2 splitting by DBDs by investigating the effect of various operating conditions. We found that tuning the power versus gas flow rate can increase the conversion and energy efficiency at a certain SEI, but this is only observed for high values of SEI (above 100 J cm^{-3}), which yields a low energy efficiency. A decrease of the discharge gap can enhance the filament formation, and therefore, the conversion and energy efficiency, but this enhancement was only observed for larger gaps. Changing the dielectrics from quartz to alumina did not show any effect on the conversion and energy efficiency, although more sophisticated dielectric materials did show drastic changes.[4–6, 39, 40]

We compare our results with those of studies published for CO_2 splitting by several types of plasmas as well as with classical thermal splitting (Table 2). We can only compare with other studies for pure CO_2 splitting as other gas mixtures (e.g., with inert gases) affect the conversion and energy efficiency,[4, 5, 27, 37–40, 61] and we do not want to draw the wrong conclusions. We focus on the maximum conversion, the energy efficiency (if this could be calculated from the literature data), and the gas flow rate. The latter is also relevant because it gives an idea about the scalability and industrial applicability of the process. Indeed, a high conversion at a very low flow rate and long residence time is not of interest for industrial applications.

Detailed systematic studies for CO_2 splitting in a pure CO_2 mixture with values for both conversion and energy efficiency in a DBD are very scarce in the literature. The most detailed studies to date were presented by Paulussen et al.[1] and Yu et al.[2] Paulussen et al.[1] found a maximum conversion of 30% at a flow rate of 0.05 L min^{-1}, a power density of 15 W cm^{-3}, and a frequency of 60 kHz. However, they did not report the plasma power or the energy efficiency. Yu et al.[2] reported a maximum conversion of 12.5% at a constant flow rate of 40 mL min^{-1}, which is somewhat lower than our results. Their maximum energy efficiency was around 3.5%, which is also somewhat lower than that in our case. However, we should point out that the reactor used in their work had a very large gap (4 mm) to study the effect of a packing material. Therefore, we should compare these results with our results for a gap of 3.3 mm (Figure 3), which shows a maximum conversion of 25% and a maximum energy efficiency of 6%.

A microwave discharge seems very promising for CO_2 splitting.[7, 12, 13, 15, 36 50] In the 1970s, Fridman reported energy efficiencies up to 80–90% in the supersonic flow regime with a flow rate in the order of 5–50 mL min^{-1} and a static pressure between 0.02 and 0.05 atm.[7] The highest energy efficiency reported recently under similar conditions was around 60%.[13] However, these results were obtained at reduced pressure (0.2 bar), which is not practical for the high-throughput processing of exhaust gases and it will increase the total energy cost as higher pressures are required for gas storage. Furthermore, it was also reported[8, 12, 15] that increasing the pressure can lead to a significant decrease in the energy efficiency. Therefore, in this comparison, we want to look at microwave results obtained at atmospheric pressure, which allows a fairer comparison for industrial purposes. Therefore, the values listed in Table 2 apply to results obtained at 1 atm. At a pressure of 1 atm, Spencer and Gallimore[15] reported a conversion of 45% at a flow rate of 1 L min^{-1} and an energy efficiency of 20% at a flow rate of 16 L min^{-1} for a microwave discharge, which is much better than obtained for a DBD.

Another very promising discharge type for CO_2 splitting is a gliding arc plasma, in which high flow rates are possible under atmospheric conditions together with high energy efficiency and reasonable conversion.[8, 16] Nunally et al.[8] reported conversions of 2–9% for an SEI variation from 0.1–1.0 eV molecule^{-1} and a flow rate input variation in the range of 14–40 L min^{-1}. Furthermore, a maximum energy efficiency of 43% was reached at a flow rate of 27 L min^{-1}. Indarto et al.[16] obtained conversions of 15–18% at flow rates of 0.8–2.4 L min^{-1} but they did not report the energy efficiency as defined by Fridman.[7] However, they compared the power efficiency with a that of a DBD and found that the power effi-

Table 2. Comparison of our results in terms of maximum conversion and energy efficiency, and the corresponding gas flow rates in both cases, with data from the literature for other plasma types and classical thermal splitting performed at atmospheric pressure.

Plasma	Max. conversion [%]	Flow rate [L min^{-1}]	Max. energy efficiency [%]	Flow rate [L min^{-1}]
our work	35	0.01	8	0.5
DBD[1]	30	0.05	–	–
DBD[2]	12.5	0.04	3.5	0.04
microwave plasma[15]	45	1	20	16
gliding arc plasma[12]	9	14	43	27
gliding arc plasma[24]	18	0.8	–	–
thermal splitting[67]	22	0.02	–	–

ciency increased by a factor of three compared to that of the DBD described by Wang et al.[37]

We can also compare the plasma-based CO_2 splitting with classical thermal splitting in membrane reactors. In this case, high temperatures of 1400–1800 °C need to be used.[62] This illustrates the advantages of plasma technology because it can circumvent the difficult thermodynamics of this reaction. Indeed, a high temperature is not needed because the electrons are heated by the electric power and they induce the chemical reactions, whereas the gas itself can remain at or near room temperature. However, processing at high temperature can also have benefits if the thermal process is coupled to a secondary process. For instance, Jin et al.[63] proposed the coupling of CO_2 splitting and the partial oxidation of methane in a membrane reactor in such a way that the O_2 produced in the splitting diffuses to the second reactor for the partial oxidation process. This method allows the transfer of thermal energy to the membrane and to the partial oxidation process. Although this process still suffers from problems such as the instability of the membrane, sealing, and pressure drop, it shows promising results. If the stability of such membranes can be improved, new possibilities can be found, for example, in the coupling of a plasma reactor with a partial oxidation reactor, especially for gliding arc and microwave discharges, as they operate at a higher temperature.

Finally, we also looked at photo- and electrocatalytic processes, but it was impossible to compare them with plasma technology in terms of conversion and energy efficiency. We believe that a combination of different processes, such as the thermochemical cycle based on Zn/ZnO[64,65] or the photochemical reduction of CO_2,[66] might give rise to the most valuable process.

Hence, we can conclude that a DBD reactor can split CO_2 with a relatively high conversion if a low flow rate is used, but the energy efficiency is still too low for commercial applications. Indeed, if the electric energy for CO_2 splitting originates from fossil fuels, an energy efficiency of 52% would be needed to ensure that less electrical energy is consumed for this process than the electricity produced from the fossil fuel combustion, or in other words, that no more CO_2 is produced in the electricity production than can be split by the plasma process.[9]

Notably, all the DBD data reported in Table 2 are for simple DBD reactors with a pure CO_2 gas flow, such as that applied in our study. However, there is still considerable room for improvement of the DBD technology as already demonstrated in the literature.[2–6,37,39,40] Indeed, an overview of different modifications applied to DBD reactors reported in literature is shown in Figure 14 presents, which shows both the absolute values of the conversion and energy efficiency reached as well as the relative changes compared to their standard setup without the modification or with a less efficient modification. As it is difficult to compare the absolute values of conversion and energy efficiency adopted from literature (because of the different operating conditions and geometries, which are not always described thoroughly), we should mainly focus on the relative changes as a result of these reactor modifications. The relative

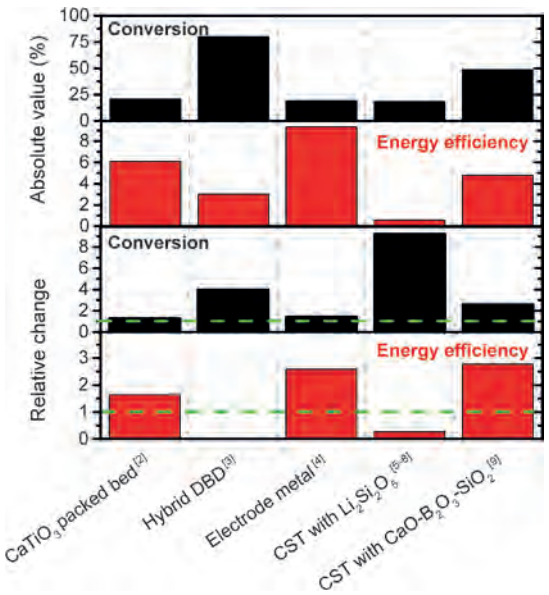

Figure 14. Modifications to a simple DBD reactor, as reported in literature, to yield a higher CO_2 conversion and energy efficiency. Both the reported maximum values of conversion and energy efficiency are plotted as well as the relative changes compared to the same setup without the modification. See text for more explanation. The dashed green line indicates no change compared to the standard setup.

changes for conversion and energy efficiency were calculated for the conditions of the highest conversion and maximum energy efficiency, respectively.

A packed-bed DBD configuration with spherical pellets was proposed by Yu et al.[2] The authors used silica gel, quartz, γ-Al_2O_3, α-Al_2O_3, and $CaTiO_3$ as packing materials and found that the maximum conversion (20.5%) was reached for $CaTiO_3$, which was a factor of 1.3 higher than for a nonpacked DBD. Furthermore, the highest energy efficiency of 6% was obtained for $CaTiO_3$, which was at least a factor 1.6 higher than that of the nonpacked DBD under the same conditions. This packing effect was attributed to the enhancement of the electron energy, which thus facilitates the electron impact dissociation of CO_2. In addition, the morphology and the acid–base properties of the packing material were found to affect the conversion. Furthermore, the presence of heterogeneous reactions on the packing surface was also identified and could facilitate the conversion. Notably, the introduction of a dielectric packing in a DBD reactor was also demonstrated to enhance the energy efficiency for volatile organic compound (VOC) remediation,[68–71] so we believe that a packed-bed DBD reactor has great potential for CO_2 splitting as well.

Tagawa et al.[3] proposed a hybrid reactor, that is, a DBD plasma on the surface of an SOEC, which allows the in situ exclusion of O_2 during CO_2 splitting. A maximum energy efficiency of 3% was reported, but we were not able to deduce the relative change of this parameter in their work. Moreover, an increase of a factor of four was observed for the conversion, up to a maximum value of 80% compared to the DBD discharge only. Indeed, a high O_2 concentration suppresses the CO_2 conversion because of its high electronegativity, which

thereby traps the electrons so that they are not available for electron impact dissociation anymore. Moreover, the oxygen will also be partially present as O atoms that can react with CO to produce CO_2. Therefore, it is logical that the in situ exclusion of O_2 has a beneficial effect on the CO_2 conversion.

Wang et al.[37] investigated the effect of different metals used as a high-voltage electrode in a DBD reactor for a mixture of 4% CO_2 in He. The advantage of the use of different metals as the central electrode is that the conductivity of the electrode changes. They obtained a relative order of Cu ≈ Au > Rh > Fe ≈ Pd ≈ Pt for the reactivity toward CO_2 decomposition, which is the same order as the electrical conductivity. A maximum conversion of 19.4% was reported for a Cu electrode, whereas the conversions for Au, Rh, Pt, Fe, and Pd were 19.2, 15.3, 14.2, 13.2, and 12.9%, respectively. We should not focus too much on these absolute values as they were obtained under other conditions (e.g., in a mixture with He). However, the relative changes are very interesting. Indeed, the Cu and Au electrodes yielded a relative increase in the conversion of a factor 1.5 compared to an Fe (stainless steel) or Pd electrode. Furthermore, a maximum energy efficiency of 9.3% was reported for the Au electrode, which was almost three times higher than the energy efficiency for the Rh electrode under the same conditions. Furthermore, we should point out that the plasma power varies between the electrodes, and therefore, the energy efficiency is the highest for Au and not for Cu. The maximum energy efficiencies for the Cu, Fe, Pd, Pt, and Rh electrodes were 8.5, 6.7, 5.9, 5.6, and 3.6%, respectively.

Li et al.[4,5,39,40] investigated the influence of $Ca_{0.8}Sr_{0.2}TiO_3$ (CST) with 0.5 wt% $Li_2Si_2O_5$ as the dielectric barrier with a mixture of 10% CO_2 in N_2. They found an improvement of the conversion by a factor of nine up to 18.5% at the same electrical power compared to silica glass as the dielectric barrier. However, if the plasma power is taken into account to calculate the theoretical energy efficiency, a decrease of the energy efficiency by a factor of 0.3 was found compared to silica glass. The authors concluded that for the same electrical power a much higher plasma power was deposited in the plasma by changing the dielectric barrier, so the actual energy efficiency is in this case closer to the theoretical energy efficiency, which was, however, only 0.6% at its maximum.

In a similar work performed by Wang et al.[6] the performance of a CST ceramic dielectric barrier with glass addition on the conversion of CO_2 was investigated. The authors produced CST ceramic barriers with the addition of $CaO\text{-}B_2O_3\text{-}SiO_2$ (CBS) glass in the range between 0.5 and 5.0 wt% to enhance the dielectric properties and the microstructures of the ceramics. The experiments were performed in a mixture of 10% CO_2 in N_2. The addition of 5.0 wt% CBS resulted in an increase of the conversion by a factor of 2.6 up to 49% compared to 0.5 wt% CBS. Furthermore, the energy efficiency almost tripled at 5.0 wt% CBS compared to that at 0.5 wt% CBS, which resulted in a maximum of 5%. The authors claimed that a higher amount of CBS leads to an increase in the total surface resistance and an increase in the capacitance of the grain boundaries, which results in a higher CO_2 conversion and a higher energy efficiency. In addition, they also found that the grain boundaries on the dielectric barrier surface serve as charge-trapping sites so that a more homogenous discharge is created.

In summary, although the absolute energy efficiencies reported in these papers are modest, the relative increase in the energy efficiencies caused by these modifications compared to a standard setup or other modifications is quite promising. Therefore, a combination of the proposed modifications with the appropriate tuning of the operating parameters might lead to even higher energy efficiencies and possibly could make a DBD reactor competitive with the other plasma systems listed in Table 2.

However, it is important to realize that more and more electrical energy nowadays originates from sustainable energy sources, and this trend will continue in coming years. In that case, the energy efficiency requirements of the plasma conversion will be somewhat less strict. Moreover, sustainable energy sources often suffer from peak currents (e.g., on sunny or windy days) when the electricity is in principle "for free". A DBD plasma can then be very useful for peak shaving, as it is very flexible and can be switched on and off easily so that it will be extremely suitable for temporary energy storage.

In general, in terms of practical use, a DBD has some benefits compared to the other plasma types (microwave and gliding arc) because its construction is simple, robust, and allows an easy scale-up, as was demonstrated 150 years ago for the commercial application of O_3 production.[7,60] Moreover, it is reported in the literature that by combining a DBD with a catalyst, in so-called plasma catalysis,[72–74] the selectivity of the process can be steered towards the desired products. This is not really an issue for pure CO_2 splitting, but it is very promising if a coreagent (e.g., methane or water) is added, to produce value-added compounds, such as syngas, methanol, formaldehyde, and formic acid.[46,72,75]

Conclusions

We investigated in detail the effect of various operating conditions on the conversion and energy efficiency of CO_2 splitting in a dielectric barrier discharge (DBD) plasma reactor. The applied frequency and the kind of dielectric (quartz or alumina) seem to have no effect on the conversion and energy efficiency. The discharge gap can have a significant effect if it gives rise to a different streamer behavior. This was observed for the gap of 3.3 mm compared to the gaps of 1.8 and 2.3 mm as visualized by Lissajous plots and current waveforms. Indeed, the 3.3 mm gap results in less streamer formation, so that the effective plasma (streamer) volume, which can contribute to the CO_2 conversion, is much smaller than the actual reactor plasma volume and results in a significantly lower CO_2 conversion and energy efficiency for the same specific energy input (SEI).

Clearly, the SEI is the most dominant factor that determines the conversion and energy efficiency. The conversion increases clearly, whereas the energy efficiency decreases, with increasing SEI, which is logical. The SEI itself is determined by both the plasma power and the gas flow rate. We observed that the gas flow rate, and hence the residence time, has the most im-

portant effect on the conversion and energy efficiency. The power has some effect, but it is less significant. Indeed, a higher power with higher gas flow rate gives rise to more intense streamers, but the residence time is lower, and the latter seems to be more important as it determines the time that the CO_2 molecules stay within the streamers and can be subject to conversion. Therefore, a lower power with lower gas flow rate results in a higher conversion and energy efficiency than a higher power with higher gas flow rate at the same fixed SEI. This is of interest because it means that a proper tuning of power versus gas flow rate can increase the conversion and energy efficiency at a certain SEI. However, we observed this behavior only for high values of SEI (above 100 J cm^{-3}), which unfortunately yield a low energy efficiency. The effect of the various parameters on the conversion and energy efficiency is summarized in Table 3.

Table 3. Summary of the experimental parameter screening to illustrate the effect of the parameters on the CO_2 conversion and energy efficiency.

Parameter	Effect on conversion	Effect on energy efficiency
lower gas flow rate/higher residence time	↑↑	↓↓
higher power	↑	↓
larger gap (if streamer formation ↓)	↓	↓
higher frequency	–	–
dielectric (alumina/quartz)	–	–

The highest CO_2 conversion was found to be around 35% and was obtained at a high SEI (above 200 J cm^{-3}), which corresponds to a low energy efficiency of only 2%. However, the highest energy efficiency of 8% was obtained at low SEI (~25 J cm^{-3}) at the expense of the conversion, which was only a few percent in this case. The selectivities of the formed products (i.e., CO and O_2) were also measured but they were always found to be around 50% under all conditions investigated.

Besides the experimental results, we have also presented modeling results for the CO_2 splitting, and reasonable agreement was obtained between the calculated and measured conversions and energy efficiencies as a function of SEI if the power density (and hence the SEI) in the model was multiplied by a factor of seven to account for the smaller volume occupied by the streamers compared to the total plasma reactor volume.

As the model shows a good correlation with the experimental trends, it can be used to elucidate the most important chemical reactions for the CO_2 splitting. For this purpose, we have reduced the chemistry set of our complete model to a simpler model with only nine species and 17 reactions to better identify the critical reactions. It was found that the CO_2 splitting is mainly dictated by electron impact dissociation (to form CO and O atoms), electron impact ionization (to form CO_2^+ ions, which will subsequently recombine with electrons or O_2^- ions into CO and O or O_2), and electron dissociative attachment (to form CO and O^- ions). The CO molecules can recombine with O^- ions or O atoms to reform CO_2, but these reactions are only important at high oxygen densities or high conversions (i.e., a long residence time). The O atoms can, however, recombine easily into O_2 by a three-body reaction, although a fraction also recombines into O_3. Furthermore, there are several other reactions between O, O_2, and O_3. Therefore, most freedom to influence the splitting process can be found in the balance of $O/O_2/O_3$.

Finally, we have compared our experimental results for the CO_2 splitting in a DBD with literature data for several types of plasma reactors as well as with classical thermal CO_2 splitting. We can conclude that a DBD reactor can provide reasonable conversions, but the energy efficiency is still too low for commercial applications, at least if electricity from fossil fuel combustion is used. However, in the literature, several modifications to a standard DBD reactor have been reported already. We have presented a summary of these reactor modifications from the literature, which illustrate that they might improve the energy efficiency, as well as the conversion.

Furthermore, if electricity from sustainable energy sources is used, the energy efficiency might be somewhat less critical. In this respect, we believe that a DBD plasma can become very useful in the future for energy storage of peak currents as it can be switched on and off easily.

Finally, a DBD reactor is also very promising in combination with catalysis. Indeed, if a catalytic packing is introduced in a DBD reactor, the selectivity of the process (in the case of a coreagent such as methane or water) can be tuned, which holds great promise for the selective production of value-added chemicals.

Experimental Section

Experimental setup

Plasma reactor

A schematic of the experimental setup, front view and top view, is shown in Figure 15. The plasma reactor is a tubular DBD reactor that consists of a dielectric tube and two concentric cylindrical electrodes. The inner electrode is a stainless-steel rod, which is grounded. We used several diameters for this inner electrode, that is, 10, 12, and 13 mm, to vary the discharge gap (see below). The outer electrode is a Ni foil, which is connected to a high-voltage power supply and placed around the dielectric tube. The latter has an inner diameter of 16.54 mm and an outer diameter of 22 mm. We used two types of dielectrics, alumina and quartz. The length of the total reactor, which includes inner electrode and dielectric tube, is 200 mm, but the length of the Ni mesh electrode was only 90 mm, and the latter defines the length of the discharge plasma.

The CO_2 gas flow to the plasma reactor was regulated by mass flow controllers (EL-flow of Bronkhorst) and can be adjusted between 10 and 1000 mL min^{-1}. The temperature of the gas was monitored at the inlet and outlet of the DBD reactor by using resistance temperature detectors (Endress-Hauser). The DBD reactor was powered by an AC high-voltage power supply (AFS), which provides a maximum peak-to-peak voltage of 40 kV and a variable frequency of 1–90 kHz. The total current was recorded by using a Rogowski-type current monitor (Pearson 4100), and a high-voltage probe (Tektronix P6015 A) was used to measure the applied

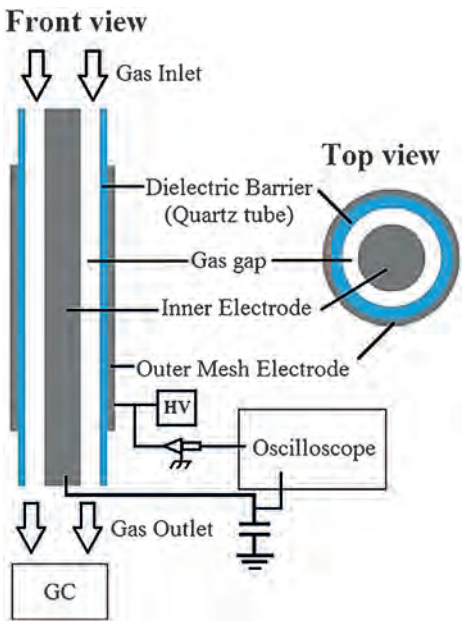

Figure 15. Schematic diagram of the experimental setup.

voltage. Furthermore, to obtain the charge generated in the discharge, the voltage on the external capacitor (10 nF) was measured. Finally, all the electrical signals were sampled by using a four-channel digital oscilloscope (PicoScope 6402A), and the discharge power was measured by means of Lissajous figures (see below).

Gas analysis

The feed and product gases were analyzed by a three-channel compact gas chromatograph (CGC; Interscience) equipped with two thermal conductivity detectors (TCD) and a flame ionization detector (FID). The first TCD channel contained a Molecular Sieve 5A column for the segregation of the molecular gases, O_2, N_2, and CO, and the second TCD channel was equipped with an Rt-QBOND column for the measurement of CO_2 and C_1–C_2 hydrocarbons. The FID was equipped with an Rtx-5 column for the measurement of C_1–C_{10}-containing compounds.

The conversion of CO_2 was calculated from the peak areas measured in the gas chromatograms, in which $CO_{2,inlet}$ is measured without plasma [Eq. (6)]:

$$X_{CO_2}[\%] = \left(\frac{CO_{2,\,inlet} - CO_{2,\,outlet}}{CO_{2,\,inlet}}\right) \times 100\% \quad (6)$$

The oxygen-based selectivities of CO and O_2 are calculated as [Eqs. (7) and (8)]:

$$S_{CO}[\%] = 0.5 \times \frac{CO_{outlet}}{CO_{2,\,inlet} - CO_{2,\,outlet}} \times 100\% \quad (7)$$

$$S_{O_2}[\%] = \frac{O_{2,\,outlet}}{CO_{2,\,inlet} - CO_{2,\,outlet}} \times 100\% \quad (8)$$

To calculate the energy cost and energy efficiency of the process, we first define the SEI in the plasma from the power and the gas flow rate [Eq. (9)]:

$$SEI\left[\frac{J}{cm^3}\right] = SEI\left[\frac{kJ}{L}\right] = \frac{Power[kW]}{Flowrate\left[\frac{L}{min}\right]} \times 60\left[\frac{s}{min}\right] \quad (9)$$

The energy cost to produce 1 mol of CO is then calculated as [Eq. (10)]:

$$E_{CO}\left[\frac{kJ}{mol}\right] = SEI\left[\frac{kJ}{L}\right] \times \frac{molar\ volume\left[\frac{L}{mol}\right] \times 100\%}{X_{CO_2}[\%]} \quad (10)$$

And finally, the energy efficiency (η) is calculated as [Eq. (11)]:

$$\eta[\%] = \frac{\Delta H_R\left[\frac{kJ}{mol}\right]}{E_{CO}\left[\frac{kJ}{mol}\right]} \times 100\% \quad (11)$$

in which the value of the reaction enthalpy (ΔH_R) is 279.8 kJ mol^{-1} (see Introduction).

A critical remark should be made if inline GC analysis is performed on plasma gas processing. If an external calibration method is used, the quantities of the gas components are defined as a function of the molar flow rate of each species. However, the latter changes during the conversion, mainly because of chemical reactions and possibly also because of deposition at the reactor walls. Pinhão and co-workers estimated an expansion (contraction) factor α for mixtures of He/CH_4/CO_2 between 0.98 and 1.12.[27] The introduction of noble gases in the gas mixture would allow for an internal calibration, which takes this variation in molar flow rate into account. However, we are interested in the CO_2 conversion without the influence of a noble gas as internal standard. Therefore, in this work, external standards are used, but to account for this expansion effect, we correct, for each specific conversion, for the change in volume caused by the change in the total number of moles. More specifically, for the reaction under study ($CO_2 \rightarrow CO + 0.5\,O_2$), this means for example, at 10% conversion, that the gas mixture contains 90 vol% CO_2, 10 vol% CO, and 5 vol% O_2, which amounts to a total of 105 vol%. So we multiply by 105% to correct for this change in volume. Of course, this assumes that no products other than CO and O_2 are formed. These are indeed the only products detected by GC.

Description of the model

The calculations were performed with a 0D chemical kinetics model, called Global kin, developed by Dorai and Kushner.[76] It calculates the spatially averaged densities of all plasma species as a function of time based on a large number of production and loss terms defined by the chemical reactions. The electron temperature is calculated with an energy balance equation, and the rate coefficients for electron impact reactions are calculated with a Boltzmann solver. Eight different neutral species (CO_2, CO, C_2O, C_2, C, O_2, O_3, and O), 11 different positive ions, six different negative ions, and the electrons are taken into account in the model. Furthermore, several excited levels of CO_2, CO, and O_2 are considered, as explained in detail by Aerts et al.[10] Hence, in total, the model consists of 42 different chemical species that react with each other in 501 chemical reactions, which include electron impact reactions, ion–ion, ion–neutral, and neutral–neutral reactions.

The equations used in the model, the entire reaction chemistry for CO_2 splitting, and the approach to mimic the filamentary character of a DBD were published in Refs. [10,59]. However, in the latter work we focused on the detailed plasma chemistry in one microdi-

scharge pulse (of 30 ns) and its afterglow, as well as five consecutive pulses, but no simulations have been performed yet for real residence times in the reactor. In the present paper, we apply this model to exactly the same residence times as obtained in the experiments, that is, in the order of 1–60 s. This means that up to 2000 consecutive pulses (of 60 ns) are simulated with an interpulse time of 0.029 s (34.4 Hz) to mimic the filamentary character of the DBD, that is, the gas molecules pass through a large number of microdischarge filaments on their way through the reactor. Notably, the time between two filaments, as "experienced" by the gas molecules, is not known. Therefore, we selected an interpulse time of 0.029 s because it yields reasonable agreement with the experiments for the conversion versus residence time. Moreover, it avoids the accumulation of the plasma species to unfeasibly high densities in subsequent pulses, which would influence the conversion if the interpulse time was too short. Furthermore, we have chosen the pulse duration to be 60 ns instead of 30 ns because this will reduce the total number of pulses required for the same SEI, and thus it reduces the calculation time. As the actual plasma volume (i.e., sum of the filament volumes) is much smaller than the total volume of the plasma reactor, the deposited energy density in the model needs to be typically a factor 10–100 higher, which depends on the gas and reactor geometry under study (i.e., filamentary character or not) to account for this smaller volume.[48,49] In our case, the deposited energy was chosen to be a factor of seven higher.

Finally, we have also developed a reduced chemistry set, by comparing the calculation results with the full set, in the entire range of conditions investigated here. This reduced set can be very useful for more time-consuming 2D or 3D plasma models of CO_2 splitting.

Acknowledgements

The authors acknowledge financial support from an IOF-SBO project of the University of Antwerp and from the IAP/7 (Interuniversity Attraction Pole) program PSI-Physical Chemistry of Plasma–Surface Interactions, supported financially by the Belgian Federal Office for Science Policy (BELSPO). The calculations were performed using the Turing HPC infrastructure at the CalcUA core facility of the Universiteit Antwerpen, a division of the Flemish Supercomputer Center VSC, funded by the Hercules Foundation, the Flemish Government (department EWI), and the Universiteit Antwerpen. Finally, we are very grateful to M. Kushner and group members for providing the Global kin code.

Keywords: carbon dioxideenergy conversion · kinetic modeling · plasma chemistry · reaction mechanisms

[1] S. Paulussen, B. Verheyde, X. Tu, C. De Bie, T. Martens, D. Petrovic, A. Bogaerts, B. Sels, *Plasma Sources Sci. Technol.* **2010**, *19*, 034015.
[2] Q. Yu, M. Kong, T. Liu, J. Fei, X. Zheng, *Plasma Chem. Plasma Process.* **2012**, *32*, 153 – 163.
[3] Y. Tagawa, S. Mori, M. Suzuki, I. Yamanaka, T. Obara, J. Ryu, Y. Kato, *Kagaku Kogaku Ronbunshu* **2011**, *37*, 114 – 119.
[4] R. Li, Q. Tang, S. Yin, T. Sato, *J. Phys. D* **2007**, *40*, 5187 – 5191.
[5] R. Li, Q. Tang, S. Yin, T. Sato, *Appl. Phys. Lett.* **2007**, *90*, 131502.
[6] S. Wang, Y. Zhang, X. Liu, X. Wang, *Plasma Chem. Plasma Process.* **2012**, *32*, 979 – 989.
[7] A. Fridman, *Plasma Chemistry*, Cambrigde University Press, New York, **2008**.
[8] T. Nunnally, K. Gutsol, A. Rabinovich, A. Fridman, A. Gutsol, A. Kemoun, *J. Phys. D* **2011**, *44*, 274009.
[9] L. F. Spencer, A. D. Gallimore, *Plasma Chem. Plasma Process.* **2011**, *31*, 79 – 89.
[10] R. Aerts, T. Martens, A. Bogaerts, *J. Phys. Chem. C* **2012**, *116*, 23257 – 23273.
[11] M. Tsuji, T. Tanoue, K. Nakano, Y. Nishimura, *Chem. Lett.* **2001**, *30*, 22 – 23.
[12] A. Vesel, M. Mozetic, A. Drenik, M. Balat-Pichelin, *Chem. Phys.* **2011**, *382*, 127 – 131.
[13] A. P. H. Goede, W. A. Bongers, M. G. Graswinckel, R. M. C. van de Sanden, L. Martina, K. Jochen, A. Schulz, W. Mathias, *3rd Eur. Energy Conf. Budapest*, **2013**.
[14] A. Indarto, J. Choi, H. Lee, H. K. Song, *Environ. Eng. Sci.* **2006**, *23*, 1033 – 1043.
[15] L. F. Spencer, A. D. Gallimore, *Plasma Sources Sci. Technol.* **2013**, *22*, 015019.
[16] A. Indarto, D. R. Yang, J.-W. Choi, H. Lee, H. K. Song, *J. Hazard. Mater.* **2007**, *146*, 309 – 315.
[17] M. Kraus, B. Eliasson, U. Kogelschatz, A. Wokaun, *Phys. Chem. Chem. Phys.* **2001**, *3*, 294 – 300.
[18] Q. Wang, B.-H. Yan, Y. Jin, Y. Cheng, *Plasma Chem. Plasma Process.* **2009**, *29*, 217 – 228.
[19] Q. Wang, H. Shi, B. Yan, Y. Jin, Y. Cheng, *Int. J. Hydrogen Energy* **2011**, *36*, 8301 – 8306.
[20] J. Sentek, K. Krawczyk, M. Młotek, M. Kalczewska, T. Kroker, T. Kolb, A. Schenk, K.-H. Gericke, K. Schmidt-Szałowski, *Appl. Catal. B* **2010**, *94*, 19 – 26.
[21] I. Istadi, N. Amin, *Chem. Eng. Sci.* **2007**, *62*, 6568 – 6581.
[22] Q. Wang, B.-H. Yan, Y. Jin, Y. Cheng, *Energy Fuels* **2009**, *23*, 4196 – 4201.
[23] H. J. Gallon, H. Kim, X. Tu, J. C. Whitehead, *IEEE Trans. Plasma Sci.* **2011**, *39*, 2176 – 2177.
[24] H. J. Gallon, X. Tu, J. C. Whitehead, *Plasma Processes Polym.* **2012**, *9*, 90 – 97.
[25] X. Tu, H. J. Gallon, M. V. Twigg, P. A. Gorry, J. C. Whitehead, *J. Phys. D* **2011**, *44*, 274007.
[26] X. Tao, M. Bai, X. Li, H. Long, S. Shang, Y. Yin, X. Dai, *Prog. Energy Combust. Sci.* **2011**, *37*, 113 – 124.
[27] N. R. Pinhão, A. Janeco, J. B. Branco, *Plasma Chem. Plasma Process.* **2011**, *31*, 427 – 439.
[28] G. Scarduelli, G. Guella, D. Ascenzi, P. Tosi, *Plasma Processes Polym.* **2011**, *8*, 25 – 31.
[29] C. De Bie, T. Martens, J. van Dijk, S. Paulussen, B. Verheyde, S. Corthals, A. Bogaerts, *Plasma Sources Sci. Technol.* **2011**, *20*, 024008.
[30] R. Snoeckx, R. Aerts, X. Tu, A. Bogaerts, *J. Phys. Chem. C* **2013**, *117*, 4957 – 4970.
[31] B. Fidalgo, A. Dominguez, J. Pis, J. Menendez, *Int. J. Hydrogen Energy* **2008**, *33*, 4337 – 4344.
[32] Z. Bo, J. Yan, X. Li, Y. Chi, K. Cen, *Int. J. Hydrogen Energy* **2008**, *33*, 5545 – 5553.
[33] M. Kano, G. Satoh, S. Iizuka, *Plasma Chem. Plasma Process.* **2012**, *32*, 177 – 185.
[34] U. Kogelschatz, *Plasma Chem. Plasma Process.* **2003**, *23*, 1 – 46.
[35] S. Futamura, H. Kabashima, *Carbon Dioxide Utilization for Global Sustainability, Proceedings of the 7th International Conference on Carbon Dioxide Utilization*, Elsevier, **2004**.
[36] A. Gutsol, A. Rabinovich, A. Fridman, *J. Phys. D* **2011**, *44*, 274001.
[37] J. Wang, G. Xia, A. Huang, S. L. Suib, Y. Hayashi, H. Matsumoto, *J. Catal.* **1999**, *185*, 152 – 159.
[38] G. Zheng, J. Jiang, Y. Wu, R. Zhang, H. Hou, *Plasma Chem. Plasma Process.* **2003**, *23*, 59 – 68.
[39] R. Li, Q. Tang, S. Yin, T. Sato, *Fuel Process. Technol.* **2006**, *87*, 617 – 622.
[40] R. Li, *Solid State Ionics* **2004**, *172*, 235 – 238.
[41] H.-H. Kim, A. Ogata, *Eur. Phys. J. Appl. Phys.* **2011**, *55*, 13806.
[42] D. R. Lide, W. M. M. Haynes, G. Baysinger, L. I. Berger, D. L. Roth, D. Zwillinger, M. Frenkel, R. N. Goldberg, *J. Am. Chem. Soc.* **2009**, *131*, 12862 – 12862.
[43] R. Valdivia-Barrientos, J. Pacheco-Sotelo, M. Pacheco-Pacheco, J. S. Benítez-Read, R. López-Callejas, *Plasma Sources Sci. Technol.* **2006**, *15*, 237 – 245.
[44] K. F. Young, H. P. R. Frederikse, *J. Phys. Chem. Ref. Data* **1973**, *2*, 313.

[45] K. Francke, R. Rudolph, H. Miessner, *Plasma Chem. Plasma Process.* **2003**, *23*, 47 – 57.
[46] D. Larkin, *Catal. Today* **2001**, *71*, 199 – 210.
[47] A. A. Khassin, B. L. Pietruszka, M. Heintze, V. N. Parmon, *React. Kinet. Catal. Lett.* **2004**, *82*, 111 – 119.
[48] O. Motret, C. Hibert, S. Pellerin, J. M. Pouvesle, *J. Phys. D* **2000**, *33*, 1493 – 1498.
[49] O. Motret, S. Pellerin, M. Nikravech, *Plasma Chem. Plasma Process.* **1997**, *17*, 393 – 407.
[50] T. Kozák, A. Bogaerts, *Plasma Sources Sci. Technol.* **2014**, *23*, 045004.
[51] T. G. Beuthe, J.-S. Chang, *Jpn. J. Appl. Phys.* **1997**, *36*, 4997 – 5002.
[52] A. Cenian, A. Chernukho, V. Borodin, *Contrib. Plasma Phys.* **1995**, *35*, 273 – 296.
[53] A. A. Ionin, I. V. Kochetov, A. P. Napartovich, N. N. Yuryshev, *J. Phys. D* **2007**, *40*, R25 – R61.
[54] H. Hokazono, H. Fujimoto, *J. Appl. Phys.* **1987**, *62*, 1585.
[55] H. Hokazono, M. Obara, K. Midorikawa, H. Tashiro, *J. Appl. Phys.* **1991**, *69*, 6850.
[56] S. Hadj-Ziane, B. Held, P. Pignolet, R. Peyrous, C. Coste, *J. Phys. D* **1992**, *25*, 677 – 685.
[57] A. Cenian, A. Chernukho, V. Borodin, G. Śliwiński, *Contrib. Plasma Phys.* **1994**, *34*, 25 – 37.
[58] W. Tsang, R. F. Hampson, *J. Phys. Chem. Ref. Data* **1986**, *15*, 1087 – 1279.
[59] R. Aerts, R. Snoeckx, A. Bogaerts, *Plasma Processes Polym.* **2014**, *11*, 985 – 992.
[60] B. Eliasson, M. Hirth, U. Kogelschatz, *J. Phys. D* **1987**, *20*, 1421 – 1437.
[61] M. Ramakers, I. Michielsen, R. Aerts, V. Meynen, A. Bogaerts, unpublished results.
[62] S. Rayne, *Nat. Preced.* **2008**, DOI: 10.1038/npre.2008.1741.1.
[63] W. Jin, C. Zhang, P. Zhang, Y. Fan, N. Xu, *AIChE* **2006**, *52*, 2545 – 2550.
[64] M. E. Gálvez, P. G. Loutzenhiser, I. Hischier, A. Steinfeld, *Energy Fuels* **2008**, *22*, 3544 – 3550.
[65] P. G. Loutzenhiser, M. E. Gálvez, I. Hischier, A. Stamatiou, A. Frei, A. Steinfeld, *Energy Fuels* **2009**, *23*, 2832 – 2839.
[66] R. D. Richardson, E. J. Holland, B. K. Carpenter, *Nat. Chem.* **2011**, *3*, 301 – 303.
[67] Y. Nigara, B. Cales, *Bull. Chem. Soc. Jpn.* **1986**, *59*, 1997 – 2002.
[68] H. L. Chen, H. M. Lee, S. H. Chen, *Ind. Eng. Chem. Res.* **2008**, *47*, 2122 – 2130.
[69] G. Horvath, N. J. Mason, L. Polachova, M. Zahoran, L. Moravsky, S. Matejcik, *Plasma Chem. Plasma Process.* **2010**, *30*, 565 – 577.
[70] A. Ogata, K. Mizuno, S. Kushiyama, T. Yamamoto, *Plasma Chem. Plasma Process.* **1998**, *18*, 363 – 373.
[71] H.-X. Ding, A.-M. Zhu, X.-F. Yang, C.-H. Li, Y. Xu, *J. Phys. D* **2005**, *38*, 4160 – 4167.
[72] X. Tu, J. C. Whitehead, *Appl. Catal. B* **2012**, *125*, 439 – 448.
[73] K. Francke, *Catal. Today* **2000**, *59*, 411 – 416.
[74] H. Chen, H. Lee, S. Chen, Y. Chao, M. Chang, *Appl. Catal. B* **2008**, *85*, 1 – 9.
[75] T. Nozaki, K. Okazaki, *J. Jpn. Pet. Inst.* **2011**, *54*, 146 – 158.
[76] R. Dorai, M. J. Kushner, *J. Appl. Phys.* **2000**, *88*, 3739 – 3747.

Received: August 12, 2014
Revised: November 14, 2014
Published online on January 9, 2015